0022-3565/09/3282-652–662$20.00
THE JOURNAL OF PHARMACOLOGY AND EXPERIMENTAL THERAPEUTICS

JPET 328:652–662, 2009

Vol. 328, No. 2
146647/3429080
Printed in U.S.A.

Physiologically Based Pharmacokinetic Modeling to Predict Transporter-Mediated Clearance and Distribution of Pravastatin in Humans

Takao Watanabe, Hiroyuki Kusuhara, Kazuya Maeda, Yoshihisa Shitara, and Yuichi Sugiyama

Department of Molecular Pharmacokinetics, Graduate School of Pharmaceutical Sciences, The University of Tokyo, Tokyo, Japan (T.W., H.K., K.M., Y.Su.); and Department of Biopharmaceutics, Graduate School of Pharmaceutical Sciences, Chiba University, Chiba, Japan (Y.Sh.)

Received September 25, 2008; accepted November 7, 2008

ABSTRACT

Hepatobiliary excretion mediated by transporters, organic anion-transporting polypeptide (OATP) 1B1 and multidrug resistance-associated protein (MRP) 2, is the major elimination pathway of an HMG-CoA reductase inhibitor, pravastatin. The present study examined the effects of changes in the transporter activities on the systemic and liver exposure of pravastatin using a physiologically based pharmacokinetic model. Scaling factors, determined by comparing in vivo and in vitro parameters of pravastatin in rats for the hepatic uptake and canalicular efflux, were obtained. The simulated plasma and liver concentrations and biliary excretion profiles were very close to the observed data in rats under linear and nonlinear conditions. In vitro parameters, determined in human cryopreserved hepatocytes and canalicular membrane vesicles, were extrapolated to in vivo parameters using the scaling factors obtained in rats. The simulated plasma concentrations of pravastatin were close to the reported values in humans. Sensitivity analyses showed that changes in the hepatic uptake ability altered the plasma concentration of pravastatin markedly but had a minimal effect on the liver concentration, whereas changes in the ability of canalicular efflux altered the liver concentration of pravastatin markedly but had a small effect on the plasma concentration. In conclusion, the model allows the prediction of the disposition of pravastatin in humans. The present study suggests that changes in the OATP1B1 activities may have a small and a large impact on the therapeutic efficacy and side effect (myopathy) of pravastatin, respectively, whereas those in the MRP2 activities may have opposite impacts (i.e., large and small impacts on the therapeutic efficacy and side effect).

Predicting the disposition of drugs in humans, particularly in the early stages of drug development, has been a critical issue in selecting the proper candidate drugs because the exposure of drugs to target organs is the major factor determining their pharmacological and/or toxicological activity. Human liver microsomes allow the reliable prediction of the metabolic clearance of drugs in humans (Rane et al., 1977; Iwatsubo et al., 1997; Obach, 1999; Naritomi et al., 2001). Biliary excretion, another hepatic elimination pathway, is the major systemic elimination pathway, particularly for amphipathic anionic drugs such as HMG-CoA reductase inhibitors (statins) and angiotensin II receptor antagonists. Because multiple transporters on the sinusoidal and canalicular membranes are involved, it is necessary to separately determine three kinetic parameters: 1) uptake, 2) sinusoidal efflux, and 3) canalicular efflux, to predict biliary clearance with regard to the plasma concentration (Giacomini and Sugiyama, 2005; Shitara et al., 2006a). The uptake clearance determined in freshly isolated rat hepatocytes correlates well with that determined with the multiple indicator dilution method (Miyauchi et al., 1993), and rat hepatocytes are reported to be a useful tool for predicting the hepatic clearance of drugs with significant hepatic uptake (Soars et al., 2007). Although cryopreserved human hepatocytes and canalicular membrane vesicles (CMVs) are commercially available, their usefulness in predicting in vivo hepatic up-

Article, publication date, and citation information can be found at http://jpet.aspetjournals.org.
doi:10.1124/jpet.108.146647.

ABBREVIATIONS: CMV, canalicular membrane vesicle; PBPK, physiologically based pharmacokinetic; OATP, organic anion-transporting polypeptide; MRP, multidrug resistance-associated protein; SF, scaling factor; R-122798, (3*R*,5*R*)-3,5-dihydroxy-7-[(1*S*,2*S*,6*S*,8*S*,8a*R*)-6-hydroxy-8-(isobutyryloxy)-2-methyl-1,2,6,7,8,8a-hexahydronaphthalen-1-yl]heptanoic acid; LC/MS, liquid chromatography/mass spectrometry; PS, permeability surface product; inf, influx; dif, diffusion; CL, clearance; met, metabolism; tot, total; B, blood; AUC, area(s) under the concentration-time curve.

take and canalicular efflux clearance remains to be examined. No method to quantify in vitro sinusoidal efflux has yet been established.

A physiologically based pharmacokinetic (PBPK) model, in which compartments representing tissues are connected with the blood flow, has been used to predict the time profiles of plasma and tissue concentrations (Kawai et al., 1998; Jones et al., 2006). The PBPK model is quite useful for simulating the effects of drug-drug interactions and genetic variations in drug-metabolizing enzymes and transporters on the exposure of drugs to the blood and organs and, ultimately, their effects on the pharmacological actions of drugs (Jones et al., 2006; Shitara and Sugiyama, 2006a). The purpose of this study was to establish a PBPK model to describe the disposition of pravastatin for which transporters are deeply involved in its hepatobiliary transport. Pravastatin, one of the statins used for the treatment of hyperlipidemia, was selected as the model compound in this study. The liver is a target organ for the pharmacological actions of statins, whereas myotoxic adverse effects, sometimes severe, including myopathy or rhabdomyolysis, are associated with the use of statins. Therefore, it is very important to simulate the exposure of statins to the liver and skeletal muscle to predict their pharmacological and toxicological effects. Hepatobiliary transport is the main elimination pathway of pravastatin from the systemic circulation and is mediated by uptake and efflux transporters in the liver (Shitara and Sugiyama, 2006b). The hepatic uptake of pravastatin is mainly mediated by organic anion-transporting polypeptide (OATP) 1B1, and its biliary excretion is predominantly mediated by multidrug resistance-associated protein (MRP) 2 (Yamazaki et al., 1993, 1997; Nakai et al., 2001). Pravastatin undergoes urinary excretion by tubular secretion and by glomerular filtration in humans (Singhvi et al., 1990). Organic anion transporter 3 has been suggested to be responsible for the basolateral uptake of pravastatin in rats and humans (Hasegawa et al., 2002; Nakagomi-Hagihara et al., 2007), whereas the transporter involved in its luminal efflux is yet to be identified.

In this study, in vivo experiments were carried out using male rats to obtain concentration-time profiles of pravastatin in the plasma, liver, kidney, muscle, brain, and lung. The kinetic parameters for the hepatic uptake and canalicular efflux of pravastatin were determined from in vitro transport studies using freshly isolated rat hepatocytes and CMVs, respectively. In vitro-in vivo scaling factors (SFs) were obtained for the hepatic uptake and subsequent canalicular efflux of pravastatin in rats. A PBPK model was constructed to simulate the systemic and liver exposure of pravastatin in rats. Using the PBPK model, the SFs determined in rats and kinetic parameters determined using human materials, the plasma concentration-time curve of pravastatin in humans was also simulated. Finally, the effects of changes in these transporter activities, caused by genetic polymorphisms and drug-drug interactions, on the concentration profiles of pravastatin in plasma and the liver were examined using the PBPK model.

Materials and Methods

Materials

[^{3}H]Pravastatin (45.5 Ci/mmol), unlabeled pravastatin, and a pravastatin analog, R-122798, were provided by Daiichi Sankyo Co., Ltd. (Tokyo, Japan). Cryopreserved human hepatocytes and human liver S9 fractions were purchased from In Vitro Technologies (Baltimore, MD). Human liver S9 fractions were also purchased from XenoTech, LLC (Lenexa, KS) and Tissue Transformation Technology (Edison, NJ). All other chemicals and reagents were of analytical grade and were readily available from commercial sources.

Animals

Male Sprague-Dawley rats (6–7 weeks old) were purchased from Nippon SLC (Hamamatsu, Japan). All animals were maintained under standard conditions with a reversed light/dark cycle and were treated humanely. Food and water were available ad libitum. The studies were carried out in accordance with the guidelines of the Institutional Animal Care Committee, Graduate School of Pharmaceutical Sciences, The University of Tokyo, Tokyo, Japan.

Animal Experiments

Male Sprague-Dawley rats, weighing approximately 250 to 320 g, were used throughout the experiments. Under ether anesthesia, the femoral artery was cannulated with a polyethylene catheter (SP-31) for the collection of blood samples. The bile duct was cannulated with a polyethylene catheter (PE-10) for bile collection, and the bladder was cannulated with a silicon catheter to collect urine. The femoral vein or the duodenum was cannulated with a polyethylene catheter (SP-31) for the administration of pravastatin. Each rat was placed in a Bollman cage and allowed to recover from the anesthesia before the experiments were continued. The rats were given pravastatin intravenously at 0.2, 1, 10, 50, or 200 mg/kg or intraduodenally at 20 mg/kg. Blood samples were collected at the designated times and centrifuged at 1500*g* for 10 min at 4°C to obtain plasma. Bile and urine samples were collected in preweighed test tubes at the designated intervals throughout the experiment. After the last blood sample had been taken, each rat was killed, and the liver, kidney, brain, lungs, and skeletal muscle were excised immediately for the tissue distribution study. The tissues were weighed and flash frozen in liquid nitrogen. All the samples were stored at −20°C until quantification.

Transport Study Using Human Cryopreserved Hepatocytes

This experiment was performed as described previously (Shitara et al., 2003). In brief, immediately before the study, the hepatocytes were thawed at 37°C. After they had been washed twice with ice-cold Krebs-Henseleit buffer, the cells were resuspended in Krebs-Henseleit buffer to a cell density of 1.0×10^6 viable cells/ml for the uptake study. After preincubation of the cells (1.2×10^5 cells/reaction) at 37°C for 3 min, drug uptake was initiated by the addition of labeled and unlabeled substrates to the cell suspension. The reaction was terminated after 0.5 or 2 min by separating the cells from the substrate solution. For this purpose, an aliquot of 100 μl of incubation mixture was placed in a centrifuge tube (450 μl) containing 50 μl of 2 N NaOH under a layer of 100 μl of oil (density = 1.015, a mixture of silicone oil and mineral oil; Sigma-Aldrich, St. Louis, MO). The sample tube was centrifuged for 10 s in a tabletop centrifuge (10,000*g*; Beckman Microfuge E; Beckman Coulter, Fullerton, CA). After overnight incubation in alkali to dissolve the hepatocytes, the centrifuge tube was cut, and each phase was transferred to a scintillation vial. The phase containing the dissolved cells was neutralized with 50 μl of 2 N HCl, mixed with scintillation cocktail, and its radioactivity was measured in a liquid scintillation counter (LS6000SE; Beckman Coulter). The time course for the uptake of [^{3}H]pravastatin into hepatocytes was expressed as the uptake volume (microliters per 10^6 viable cells) of the radioactivity taken up into the cells (disintegrations per minute per 10^6 cells) divided by the concentration of radioactivity in the incubation buffer (disintegrations per minute per microliter). The initial uptake velocity of [^{3}H]pravastatin was calculated from the slopes of the uptake volume versus time plots

obtained at 0.5 and 2 min and expressed as the uptake clearance (microliters per minute per 10^6 cells).

Metabolism Study Using the Liver S9 Fraction

It has been reported that pravastatin is metabolized by sulfotransferase in male rats (Kitazawa et al., 1993). Therefore, we used the liver S9 fraction as the enzyme source. The liver S9 fraction was prepared from four rats using standard procedures and stored at −80°C until use. The protein concentration was determined by the Lowry method, using bovine serum albumin as the standard. Pravastatin was incubated with a reaction mixture consisting of rat liver S9 fraction (final concentration, 8 mg/ml), NADPH-generating system (0.8 mM $NADP^+$, 8 mM glucose 6-phosphate, 1 U/ml glucose-6-phosphate dehydrogenase, and 3 mM $MgCl_2$), and 3'-phosphoadenosine 5'-phosphosulfate (final concentrations, 0.5 and 5 mM for low and high pravastatin concentrations, respectively) in the presence of 100 mM phosphate buffer, pH 7.4. After preincubation at 37°C for 10 min, pravastatin (final concentration, 0.1–500 μM) was added to initiate the enzyme reaction. At the designated time, the reactions were terminated by mixing them with equal volumes of methanol containing R-122798, an analytical internal standard, followed by centrifugation at 15,000*g* for 10 min at 4°C. The supernatant was subjected to liquid chromatography/mass spectrometry (LC/MS) analysis. In studies with the human liver S9 fraction, the concentrations of pravastatin and 3'-phosphoadenosine 5'-phosphosulfate were 5 μM and 1 mM, respectively; other incubation conditions were the same as in the rat studies.

LC/MS Analysis

Liver, kidney, brain, lung, and skeletal muscle were added to 3 to 5 volumes of physiological saline (w/v) and homogenized. Tissue homogenates and plasma, bile, and urine samples were deproteinated with 2 volumes of methanol containing the internal standard (1 μg/ml R-122798) and centrifuged at 15,000*g* for 10 min at 4°C. High-concentration samples were diluted appropriately with blank matrix before deproteination. The supernatant was subjected to LC/MS analysis. The appropriate standard curves were prepared in the equivalent blank matrix and used for each analysis.

The LC/MS consisted of an Alliance HT 2695 separation module with an autosampler (Waters, Milford, MA) and a Micromass ZQ mass spectrometer with an electron ion spray interface (Waters). The optimum operating conditions used were as follows: electrospray probe (capillary) voltage, 3.2 kV; sample cone voltage, 20 V; and source temperature, 100°C. The spectrometer was operated at a drying desolvation gas flow rate of 350 l/h. The mass spectrometer was operated in the selected ion monitoring mode using the respective MH− ions, *m/z* 423.3 for pravastatin and *m/z* 409.3 for the internal standard. The mobile phase used for high-performance liquid chromatography was acetonitrile/ammonium acetate buffer (10 mM), pH 4 = 7:3 (v/v), and the flow rate was 0.3 ml/min. Chromatographic separation was achieved on a C18 column (Inertsil ODS-3 column, 50 × 2.1 mm; particle size, 3 μm) (GL Sciences, Tokyo, Japan).

Data Analysis of Metabolic Clearance in Liver S9

The metabolic velocity was calculated from the slope of the natural log (concentration)-time plot. Because the Eadie-Hofstee plot showed curvature, the kinetic parameters were obtained using eq. 1:

$$v = \frac{V_{max1} \times S}{K_{m1} + S} + \frac{V_{max2} \times S}{K_{m2} + S} \quad (1)$$

where v is the initial velocity (picomoles per minute per milligram of protein), S is the substrate concentration (micromolar), V_{max1} and V_{max2} are the maximum velocities (picomoles per minute per milligram of protein), and K_{m1} and K_{m2} are the Michaelis constants (micromolar). Fitting was performed with the nonlinear least-squares method using the MULTI program (Yamaoka et al., 1981). The input data were weighted as the reciprocals of the observed values, and the Damping Gauss-Newton algorithm was used for fitting.

Model Development

The PBPK model was constructed to describe the pharmacokinetics of pravastatin in rats and humans (Fig. 1). The key features of this model are as follows. 1) Active uptake (PS_{inf}) and passive diffusion clearances (PS_{dif}) on the sinusoidal membrane, and biliary clearance (PS_{bile}) on the canalicular membrane in the liver are incorporated. 2) The liver compartment consists of five units of extracellular and subcellular compartments, connected by blood flow in tandem, to fit the hepatic disposition to the "dispersion" model. Because the hepatic elimination of pravastatin in rats is blood flow limited, the dispersion model is the appropriate model for the hepatic elimination of such high-clearance drugs (Roberts and Rowland, 1986; Iwatsubo et al., 1997; Naritomi et al., 2001). The number of liver compartments was determined by comparing the hepatic availability ($F_{h,n}$) and F_h predicted using the dispersion model. $F_{h,n}$ is the product of the availability in the liver compartments (eq. 2).

$$F_{h,n} = (Q/(Q + f_B(CL_{int,all}/n)))^n \quad (2)$$

where n represents the number of compartments. The integer number n, which gave the $F_{h,n}$ value closest to that in the dispersion model, was selected. 3) The brain and muscle, target tissues for the adverse effects of statins, were included. 4) Although urinary excretion is a minor elimination pathway in male rats, the kidney was included because the kidney/blood concentration ratio for pravastatin is high in male rats, probably because of the efficient uptake and/or reabsorption of pravastatin. The renal clearance of pravastatin in male rats was lower than the glomerular filtration rate corrected by the blood unbound fraction. In contrast, renal clearance must be taken into consideration in humans. Because this study focused on hepatobiliary transport, renal elimination occurs from the systemic compartment. 5) The rapid equilibrium distribution of pravastatin between the blood and tissues other than the liver was assumed. 6) The initial distribution volume, estimated by fitting the plasma concentration time profiles of pravastatin in rats after the

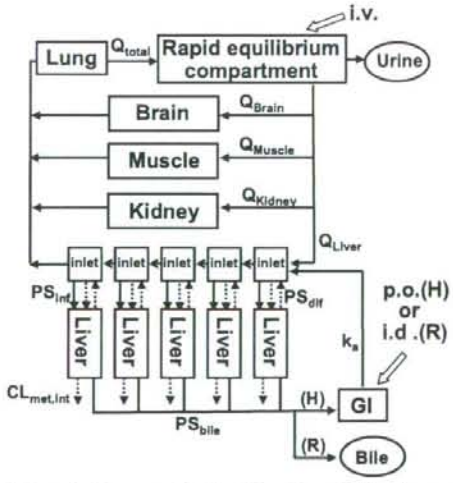

Fig. 1. Schematic diagram of the PBPK model predicting the concentration-time profiles of pravastatin. The liver compartment was divided into five compartments to mimic the dispersion model. Indicated are the blood flow (Q), the active hepatic uptake clearance (PS_{inf}), the passive diffusion clearance (PS_{dif}), the biliary clearance (PS_{bile}), and the metabolic clearance ($CL_{met,int}$), human (H), and rat (R). The enterohepatic circulation was incorporated in the case of humans.

intravenous administration of 0.2 and 1 mg/kg to a two-compartment model, was used as the volume of the rapid equilibrium compartment including the blood compartment, and it was assumed that there is no interspecies difference in the initial distribution volume. The differential equations are shown in Appendix I, and all simulations were performed with SAAM II (SAAM Institute, Seattle, WA).

Estimation of Kinetic Parameters Used in the Simulation

In Vitro Parameters (Rats and Humans). The in vitro active uptake ($PS_{inf,vitro}$) and passive diffusion clearances ($PS_{dif,vitro}$) of pravastatin on the sinusoidal membrane were determined from the uptake studies using isolated hepatocytes. The parameters for rats were taken from previous reports (Yamazaki et al., 1993; Ishigami et al., 1995), and those for humans were determined in the present study. $PS_{inf,vitro}$ and $PS_{dif,vitro}$ were regarded as the saturable and nonsaturable components, respectively, in the uptake clearance into hepatocytes. A physiological scaling factor of 1.2×10^8 cells/g liver was used for scaling up to the organ level (Iwatsubo et al., 1997). The in vitro biliary clearance ($PS_{bile,vitro}$) of pravastatin was calculated from the ATP-dependent uptake clearance into the CMVs using eq. 3 (Niinuma et al., 1999):

$$PS_{bile,vitro} = (V_{initial} \times R)/(E \times IO) \quad (3)$$

where $V_{initial}$ represents the velocity of the initial ATP-dependent uptake by CMVs corrected by medium concentration (6.08 μl/min/mg protein for rats and 1.90 μl/min/mg protein for humans), R represents the recovery of liver homogenate protein (174 mg homogenate protein/g liver for rats and 133 mg homogenate protein/g liver for humans), E represents the enrichment of the CMV fraction (70.4 for rats and 61.8 for humans), and IO represents the population of inside-out CMVs (0.347 for rats and 0.555 for humans).

In Vivo Parameters (Rats). The in vivo intrinsic biliary clearance ($PS_{bile,vivo}$) at the canalicular membrane was calculated by dividing the biliary excretion rate by the hepatic unbound concentration at steady state (Yamazaki et al., 1996b, 1997). Systemic elimination other than biliary excretion was regarded as the hepatic metabolism because renal elimination in male rats is negligible. Thus, in vivo intrinsic metabolic clearance ($CL_{met,int,vivo}$) was obtained with eq. 4:

$$CL_{met,int,vivo} = PS_{bile,vivo} \times \frac{100 - (\%\text{ of excretion into bile at 0.2mg/kg})}{(\%\text{ of excretion into bile at 0.2mg/kg})} \quad (4)$$

The in vivo passive diffusion clearance on the sinusoidal membrane was assumed to be the same as $PS_{dif,vitro}$. The in vivo active uptake clearance ($PS_{inf,vivo}$) was estimated using eq. 5:

$$PS_{inf,vivo} = CL_{int,all} \times \frac{PS_{dif,vivo} + PS_{bile,vivo} + CL_{met,int,vivo}}{PS_{bile,vivo} + CL_{met,int,vivo}} - PS_{dif,vivo} \quad (5)$$

where $CL_{int,all}$ represents the overall hepatic intrinsic clearance estimated from the hepatic availability using the dispersion model, with a dispersion number of 0.17, which was obtained by dividing the bioavailability by the fraction absorbed (Komai et al., 1992), assuming negligible metabolism in the small intestine. The average of the tissue/blood concentration ratios at 30, 60, and 90 min after the intravenous administration at 10 mg/kg pravastatin were used as the tissue/blood partition coefficient (K_p), assuming a pseudo-steady state (Table 2). Actually, the tissue/blood concentration ratios at 30, 60, and 90 min were similar (muscle, 0.28, 0.21, and 0.18; brain, 0.045, 0.029 and 0.034; kidney, 13, 14, and 15; lung, 0.76, 0.67, and 0.77 at 30, 60, and 90 min, respectively). The absorption rate constants were estimated by noncompartment analysis using the plasma concentration data.

Results

In Vivo Pharmacokinetics of Pravastatin in Rats. Figure 2 shows time profiles of the plasma concentration of pravastatin after its intravenous (0.2 mg/kg) and intraduodenal (20 mg/kg) administration and the cumulative amount of pravastatin excreted into the bile. The total blood clearance ($CL_{tot,B}$) was similar to the hepatic blood flow rate. The bioavailability of pravastatin after intraduodenal administration was calculated to be 0.0087 by comparing the AUC for pravastatin after intravenous and intraduodenal administration. Forty-six percent of the dose was recovered in the bile as the parent compound after intravenous administration, whereas the amount excreted into the urine was less than 4% of the dose. Even after intraduodenal administration, 33% was recovered in the bile.

The nonlinearity of the disposition of pravastatin was examined. The plasma concentrations and cumulative amounts excreted into the bile after its intravenous administration were determined at doses ranging from 0.2 to 200 mg/kg (Fig. 3). $CL_{tot,B}$ was independent of the dose up to 50 mg/kg but decreased to 27 ml/min/kg at 200 mg/kg pravastatin. The cumulative biliary excretion increased slightly from 46 to 60% at doses above 0.2 mg/kg and was significantly delayed at 200 mg/kg.

Hepatic Metabolism of Pravastatin in Rats. The metabolism of pravastatin in the liver was examined using S9 fractions prepared from rat liver. It exhibited biphasic kinetics with high-affinity (K_{m1}, 0.846 ± 0.403 μM; V_{max1}, 4.47 ± 1.92 pmol/mg/min) and low-affinity (K_{m2}, 80.3 ± 12.6 μM; V_{max2}, 240 ± 16.2 pmol/mg/min) components (mean ± S.D.). The sum of the in vitro metabolic clearance for the high- and low-affinity components, corrected with the physiological scaling factor of 96.1 mg protein/g liver, was used as the in

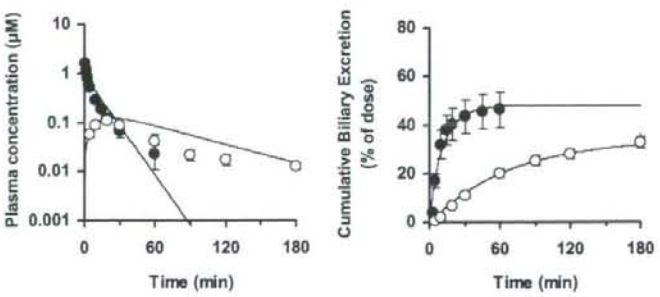

Fig. 2. Simulated and observed plasma concentrations and biliary excretion rates for pravastatin in rats after intravenous (●, 0.2 mg/kg) or intraduodenal (○, 20 mg/kg) administration. The symbols and solid lines represent experimentally observed and simulated values, respectively. Each point represents the mean ± S.E. (n = 3).

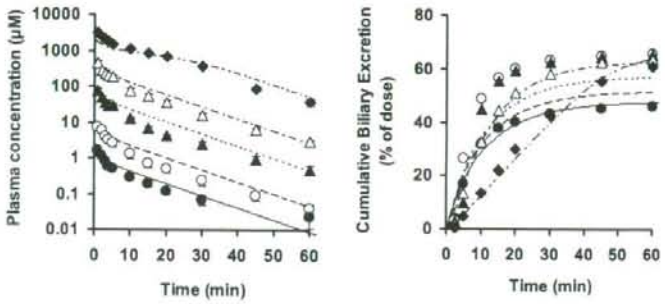

Fig. 3. Simulated and observed plasma concentrations and biliary excretion rates for pravastatin in rats after the intravenous administration of various doses. The symbols and lines represent experimentally observed and simulated values, respectively. Each point represents the mean ± S.E. (n = 3). ——— ●, 0.2 mg/kg; - - - - ○, 1 mg/kg; · · · · · · · · · · · ·, 10 mg/kg; — · — · — △, 50 mg/kg; — · · — · ◆, 200 mg/kg.

vitro metabolic clearance ($CL_{met,int,vitro}$), which was 0.793 ml/min/g liver (Table 1).

Simulation of Concentration-Time Profiles of Pravastatin in Rats. All parameters used in the simulation are summarized in Tables 1 and 2. The initial distribution volume was estimated to be 0.393 l/kg from the plasma concentration profile after the intravenous administration of 0.2 mg/kg pravastatin, which was used as the volume of the rapid equilibrium compartment in the model. Figures 2 and 3 show the simulated plasma concentrations and biliary excretion time profiles for pravastatin, together with the observed data after its intravenous and intraduodenal administration. To reproduce the in vivo pharmacokinetic profiles using in vitro parameters, SFs were necessary. For the in vitro-in vivo extrapolation of the transporter-mediated clearances, the ratio of the in vivo/in vitro intrinsic clearances of each process in rats was given as the SF (Table 1). Furthermore, using the K_m values, the simulated plasma concentration and biliary excretion time profiles gave similar values to the observed data, even under nonlinear conditions. This model reproduced the time profiles for pravastatin in the liver and other peripheral tissues after its intravenous administration (Figs. 4 and 5). In particular, the nonlinearity of the liver concentration-time profiles could also be simulated (Fig. 4). Although the model reasonably describes the experimental data, the simulated lines showed some deviation from the observed data at the terminal phase in Figs. 2 (left) and 5. This may be caused by the lack of a compartment corresponding to the organ, which is associated with the terminal phase of systemic pravastatin. Moreover, the simulation results of biliary excretion of pravastatin administered at 1 and 10 mg/kg showed some deviation from the observed data (Fig. 3, right). Because hepatic metabolism is saturated at these doses, this may be attributed to the deviation of the K_m value for metabolism.

Prediction of Pharmacokinetics in Humans. The uptake clearance determined using eight lots of human cryopreserved hepatocytes was 4.5 ± 2.9 μl/min/10^6 cells at 1 μM pravastatin and 0.77 ± 0.63 μl/min/10^6 cells at 100 μM pravastatin (mean ± S.D.). Using the physiological scaling factor of 1.2×10^8 cells/g liver, $PS_{inf,vitro,human}$ and $PS_{dif,vitro,human}$ were calculated to be 0.448 and 0.0924 ml/min/g liver, respectively (Table 1). Unlike the rat liver S9 fraction, no metabolism of pravastatin was observed up to 180 min in the human liver S9 fractions purchased from three different vendors. Thus, the hepatic metabolism of pravastatin might be negligible in the human liver. The in vivo kinetic parameters for pravastatin in humans were predicted by multiplying the corresponding in vitro parameters obtained using human materials by the SF obtained from rat studies. For PS_{bile}, the saturable (ATP-dependent) biliary clearance in humans was predicted as described above (eq. 3), and the nonsaturable component of the biliary clearance in humans was assumed to be the same as that in rats. Thus, the predicted $PS_{bile,\ vivo,\ human}$ was 0.388 ml/min/g

TABLE 1

Kinetic parameters for hepatic intrinsic clearance

Active hepatic uptake and passive diffusion clearances on the sinusoidal membrane, biliary clearance on the canalicular membrane, and metabolic clearance were estimated by both in vitro and in vivo experiments. The details of these estimations are described in the text. Values within parentheses indicate the K_m value (micromolar) for each clearance.

	Rat		Scaling Factor	Human	
	In Vitro	In Vivo		In Vitro	In Vivo*
	ml/min/g liver			*ml/min/g liver*	
PS_{inf}	2.47[a,b] (32.8)	9.06[g]	3.7	0.448	1.66
PS_{dif}	0.192[a,b]	0.192[e]	1[e]	0.0924	0.0924
PS_{bile}					
ATP-dependent	0.0433[c]	0.906[d] (92.3)	21	0.00737[c]	0.154
Nonsaturable		0.234[d]			0.234[f]
$CL_{met,int}$	0.793 (0.846, 80.3)	1.33[h]	1.7	0	0

* Predicted by multiplying the in vitro parameter by the SF.
[a] Yamazaki et al. (1993).
[b] Ishigami et al. (1995).
[c] Calculated using eq. 3 (Niinuma et al. (1999)).
[d] Yamazaki et al. (1997).
[e] Assumed that the SF for PS_{dif} is 1.
[f] Assumed negligible interspecies difference between rat and human.
[g] Calculated using eq. 5.
[h] Calculated using eq. 4.

TABLE 2
Physiological and kinetic parameters for modeling in rats and humans

	Rat	Human
Physiological Parameters		
Weight (g/kg)[a]		
Liver	41.2	24.1
Extracellular space in liver	11.5	6.7
Brain	6.8	5.3
Lung	4.0	16.7
Muscle	488	429
Kidney	9.2	4.43
Blood flow rate[a] (ml/min/kg)		
Liver	55.2	20.7
Brain	5.3	10.0
Lung	172	74.9
Muscle	30.0	10.7
Kidney	36.9	15.7
Kinetic parameters		
Plasma unbound fraction[b]	0.64	0.47
Liver unbound fraction	0.51[c]	0.51[d]
Blood/plasma ratio[e]	0.59	0.56
Fraction absorbed	0.62[f]	0.47[g]
Renal clearance (ml/min/kg)	1.5[h]	11.3[i]
Absorption rate constant (min^{-1})[j]	0.0088	0.0078
Tissue/blood concentration ratio		
Brain	0.036	0.033[k]
Lung	0.74	0.67[k]
Muscle	0.22	0.20[k]
Kidney	14	13[k]

[a] The volume and blood flow rate in each tissue were taken from Davies and Morris (1993) and Kawai et al. (1994). The tissue volume was converted to tissue weight based on the assumption that the tissue gravity is 1 g/ml.
[b] Yamazaki et al. (1996c) and manufacturer's interview form.
[c] Yamazaki et al. (1996b).
[d] Assumed negligible interspecies difference between rat and human.
[e] Yamazaki et al. (1996c) and Lennernäs and Fager (1997).
[f] Komai et al. (1992).
[g] Estimated from the bioavailability (0.18) and hepatic availability (0.38) (Singhvi et al., 1990).
[h] Obtained from the urinary excretion data for intravenous administration of 10 mg/kg.
[i] Singhvi et al. (1990).
[j] Estimated by noncompartment analysis.
[k] Estimated by $K_p = f_B/f_T$.

liver. Assuming that the distribution of pravastatin to the tissues, except the liver, occurs by passive diffusion, the tissue/blood partition coefficient (K_p) was calculated by the following equation: $K_p = f_B/f_T$, where f_B and f_T represent the blood unbound fraction (=plasma unbound fraction/blood-to-plasma concentration ratio) and the unbound fraction in the tissues, respectively. It was assumed that there is no species difference in f_T between rats and humans based on the previous report by Sawada et al. (1985). The estimated or reported physiological, anatomical, and kinetic parameters for humans used in the simulation are shown in Tables 1 and 2. Using these parameters, the plasma concentration-time profiles for pravastatin in humans after intravenous or oral administration were predicted. A lag time of 17 min was taken into consideration in the simulation of oral administration. The predicted concentration-time profiles were similar to the observed data (Fig. 6).

Effect of Transporter Activity on Systemic and Target Exposure. Sensitivity analyses were performed to understand the effects of the changes in transporter activities on the time profiles for the plasma and liver (a target organ) concentrations of pravastatin in humans. The plasma and liver concentrations after the oral administration (40 mg) of pravastatin were simulated using the PBPK model constructed in this study, with varying hepatic transport activities over a range of 0.33 to 3.0 times the initial value. The simulated concentration-time profiles and the changes in the AUC are shown in Fig. 7 and Table 3, respectively. Changes in the active hepatic uptake ability affected the plasma concentration profiles dramatically but did not greatly affect the liver concentration profiles. On the contrary, changes in the ability of canalicular efflux altered the liver concentration of pravastatin markedly but had a small effect on the plasma concentration. Changes in the passive diffusion clearance hardly affect the plasma and the liver concentration profiles.

Discussion

It is now well recognized that drug transporters play important roles in the processes of absorption, distribution, and excretion (Giacomini and Sugiyama, 2005; Shitara et al., 2006a). The purpose of this study was to construct a PBPK model to evaluate the concentration-time profiles for drugs in the plasma and peripheral organs in humans using physiological parameters, SFs, and drug-related parameters (unbound fraction and metabolic and membrane transport clearances extrapolated from in vitro experiments). The principle of the prediction was as follows. First, SFs were obtained by comparing in vitro and in vivo parameters in rats. Then, the in vitro human parameters were extrapolated in vivo using the SFs obtained in rats (Naritomi et al., 2001). Pravastatin was selected as the model compound because many studies have investigated the mechanisms involved in the drug disposition in rodents, and clinical data after intravenous and oral administration are available.

Consistent with a previous report (Yamazaki et al., 1996a), the hepatic elimination of pravastatin is blood flow limited. Considering that the maximum amount of intact pravastatin excreted into the bile was 50%, it is likely that pravastatin undergoes hepatic metabolism in rats because pravastatin is excreted negligibly in the urine. Incubating pravastatin with the rat liver S9 fractions caused a reduction in intact pravastatin with time and consisted of two different mechanisms with high- and low-affinity sites. The kinetic parameters related to hepatic clearance (PS_{inf}, PS_{dif}, PS_{bile}, and $CL_{met,int}$) were estimated from various in vivo experiments and were incorporated into the PBPK model. As a result, plasma concentration and biliary excretion-time profiles for pravastatin were successfully reproduced (Figs. 2–5). Moreover, nonlinear pharmacokinetics were also reproduced using the K_m values for hepatic uptake, biliary excretion, and metabolic clearances (Fig. 3). The liver concentrations of pravastatin were similar to the observed data,

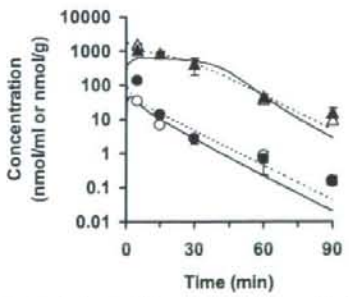

Fig. 4. Simulated and observed liver concentration profiles for pravastatin in rats after intravenous administration. Dashed and solid lines, simulated plasma and liver concentrations, respectively. Open and closed symbols, experimentally observed plasma and liver concentrations, respectively (circles, 10 mg/kg; triangles, 200 mg/kg). Each point represents the mean ± S.E. ($n = 3$).

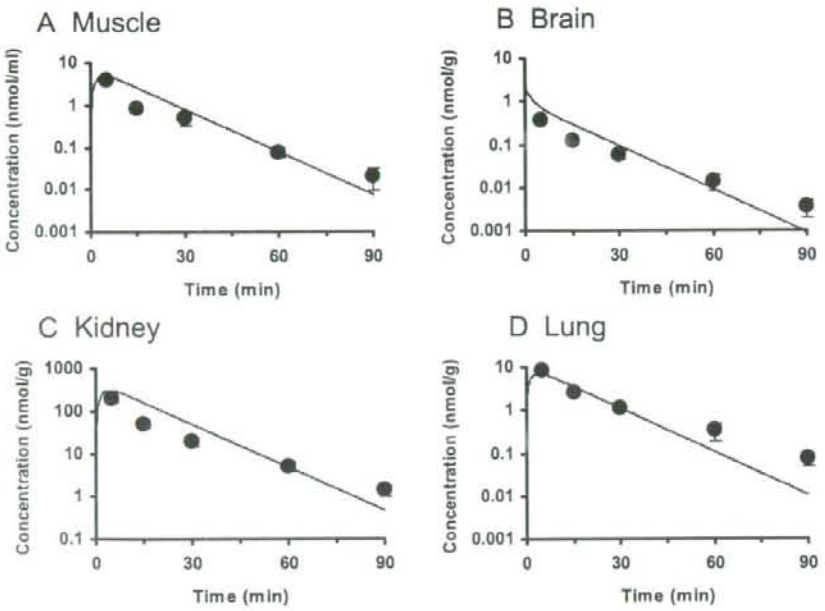

Fig. 5. Simulated and observed tissue concentration profiles for pravastatin in rats after intravenous administration at 10 mg/kg. Symbols and solid lines, experimentally observed and simulated values, respectively. Each point represents the mean ± S.E. (n = 3).

even under nonlinear conditions (200 mg/kg) (Fig. 4). These results suggest that the PBPK model constructed in this study is appropriate for describing the pharmacokinetics of pravastatin in rats.

The kinetic parameters PS_{inf}, PS_{dif}, and PS_{bile} were also determined in vitro using rat hepatocytes and CMVs to obtain the relevant SFs (Table 2). The corresponding parameters were also determined using human cryopreserved hepatocytes and CMVs. These parameters were extrapolated in vivo using the SFs determined in rats. Because there is no evidence that active transport mechanisms are involved in the sinusoidal efflux of pravastatin, the clearance corresponding to the nonsaturable component (PS_{dif}) of the uptake was used as the clearance for sinusoidal efflux. Unlike the rat liver S9 fractions, pravastatin was not metabolized in the human liver S9 fractions. Therefore, the metabolic clearance was set to zero in humans. Using the human parameters, simulated plasma concentration-time profiles of pravastatin after the intravenous and oral administration were fairly close to the observed data for humans (Fig. 6), showing that the predicted value was not far from the true value. It should be noted that the sinusoidal efflux clearance (passive diffusion clearance) was lower than the intrinsic biliary clearance with regard to the liver concentration, indicating that the hepatobiliary transport of pravastatin is likely uptake limited and that the hepatic intrinsic clearance can be approximated to PS_{inf} (Shitara et al., 2006a). Therefore, even though the predictability of the absolute values for biliary and sinusoidal efflux clearance is low, the simulated results will be close to the observed data as far as the uptake clearance is correctly predicted. To validate the predictability of those clearances, the liver concentrations must be determined in humans, which should be possible with imaging technologies such as positron emission tomography, single-photon emission computed tomography, and magnetic resonance imaging. Ghibellini et al. (2007) recently developed a methodology for the real-time measurement of the biliary excretion profiles of drugs in humans using a gamma scintigraphy technique. Further efforts are required to use such in vivo imaging technologies to increase the predictability of these pharmacokinetic parameters.

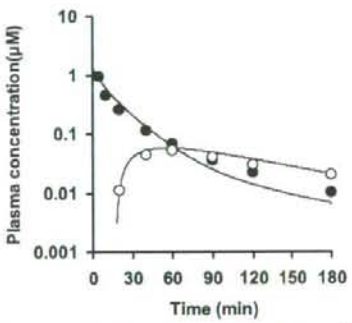

Fig. 6. Predicted and observed plasma concentration profiles for pravastatin in humans. Closed and open symbols, reported plasma concentrations after intravenous (9.9 mg) and oral (19.2 mg) administration, respectively (Singhvi et al., 1990). Solid lines, simulated values using the parameters shown in Tables 1 and 2.

To date, clinical studies have demonstrated that the genetic variations of OATP1B1 and drug-drug interactions involving OATP1B1 are associated with interindividual differences in the systemic exposure of pravastatin and other substrate drugs (Nishizato et al., 2003; Maeda et al., 2006; Niemi et al., 2006; Shitara and Sugiyama, 2006b). Because the pharmacological target of pravastatin is inside the cell, the liver exposure is a critical factor for its pharmacological activities. Based on the pharmacokinetic concepts, the AUC in the liver concentration is governed only by the sequestration clearance from the liver as far as the renal elimination is

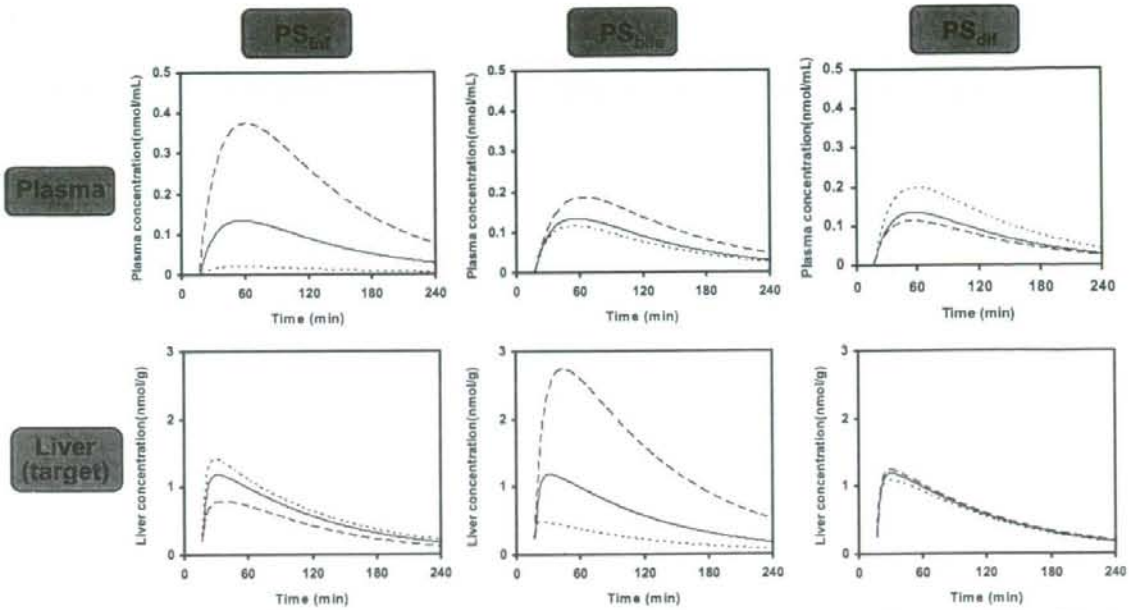

Fig. 7. Effects of changes in transporter activity on the time profiles of plasma and liver (target organ) concentrations of pravastatin in humans. Plasma and liver concentrations after oral administration (40 mg) were simulated using the PBPK model with varying hepatic transport activities over a 1/3- to 3-fold range of the initial values shown in Table 1. (———, initial; – – –, ×1/3; · · · · · · · , ×3)

negligible and is independent of the change in uptake clearance (eq. A4) (see Appendix II). When renal clearance makes a significant contribution, the changes in hepatic uptake activity can affect both the liver and the plasma AUC (Fig. 9; Appendix II). Actually, the renal elimination of pravastatin makes a significant contribution to the total body clearance (47% of the total body clearance) (Singhvi et al., 1990). Therefore, it is possible that the liver concentrations of pravastatin are affected to some extent also by the changes in the hepatic uptake activity. To support this concept, a simulation was performed with different uptake clearances (Fig. 7). Changes in the hepatic uptake clearance had a great impact on the plasma concentrations of pravastatin but less impact on the liver concentrations. In accordance, the effects of the genetic polymorphisms of OATP1B1 on the cholesterol-lowering effects of pravastatin will be small or absent at least at steady state (in other words, after relatively long-term treatment). The alteration of pharmacological effect of pravastatin with its chronic administration has not been observed in subjects with OATP1B1 polymorphisms although alteration of inhibitory effect of HMG CoA reductase activities in short-term treatments was reported (Takane et al., 2006; Kivistö and Niemi, 2007; Zhang et al., 2007). In contrast, changes in the intrinsic canalicular efflux activity should dramatically affect the liver concentration of pravastatin, whereas the plasma concentration is not affected as much by changes in the intrinsic biliary clearance (Fig. 7). Because the biliary excretion of pravastatin is mainly mediated by MRP2, the factors affecting MRP2 function, such as the use of MRP2 inhibitors or the genetic mutations causing Dubin-Johnson syndrome, will affect the pharmacological action of pravastatin. Furthermore, changes in the sinusoidal efflux clearance had only a slight impact on both the plasma and the liver concentrations. This is because, even under these conditions, the uptake process is still the rate-limiting process. Although the predictability of the sinusoidal efflux clearance remains unknown, changes within this range will not affect the simulated results.

TABLE 3

Changes in the AUC (percentage of the control) for plasma and liver concentrations of pravastatin after its oral administration when the transporter function changes

Change in Clearance	PS_{inf}		PS_{bile}		PS_{dif}	
	Plasma	Liver	Plasma	Liver	Plasma	Liver
×1	100	100	100	100	100	100
×1/3	271	68	143	255	83	103
×3	14	115	84	38	146	92

One of the serious adverse effects of statins is myopathy (rhabdomyolysis). Because its target organ is the skeletal muscle, the systemic exposure should be the determinant factor of this adverse effect. The sensitivity analyses showed that the changes in the hepatic uptake clearance had a great impact on the systemic exposure of pravastatin, whereas those in the canalicular efflux had a minimal impact (Fig. 7). The results suggest that patients with an impaired OATP1B1 might be more susceptible to pravastatin-induced myopathy than those with normal one. Morimoto et al. (2004) reported that the frequency of the OATP1B1*15 haplotype was significantly higher in patients who experienced myopathy after receiving pravastatin or atorvastatin (which is also an OATP1B1 substrate) than in patients without myopathy, and a genome-wide study elucidated that the variants in OATP1B1 are strongly associated with an increased risk of simvastatin-induced myopathy (Link et al., 2008).

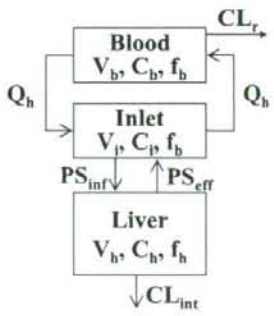

Fig. 8. Simple model to analyze the effects of changes in hepatic uptake activity and intrinsic clearance on blood and liver concentrations. Indicated are the hepatic blood flow (Q_h), renal clearance (CL_r), volume (V), concentration (C), unbound fraction (f), hepatic uptake clearance (PS_{inf}), sinusoidal efflux clearance (PS_{eff}), intrinsic clearance (CL_{int}), blood (b), inlet (i), and liver (h).

In the present study, a PBPK model, including transporter-mediated membrane transport processes, was constructed, which allows the prediction of the pharmacokinetics of pravastatin in humans. It also extends our understanding of the effects of changes in the transport processes on the pharmacological and adverse effects of drugs by simulating the exposure of the systemic circulation and tissues to them. The present study suggests that changes in the OATP1B1 activities may have a small and a large impact on the therapeutic efficacy and side effect (myopathy) of pravastatin, respectively, whereas those in the MRP2 activities may have opposite impacts (i.e., a large and a small impact on the therapeutic efficacy and side effect).

Appendix I: Differential Mass Balance Equations for the PBPK Model

Nomenclature

General. Q, blood flow rate; V, tissue weight; C, pravastatin concentration; K_p, tissue/blood partition coefficient; f_B, blood unbound fraction; f_T, tissue unbound fraction; V_m, maximum transport velocity; K_m, half-saturation concentration for transport; CL_R, renal clearance; PS_{inf}, intrinsic hepatic uptake clearance; PS_{dif}, passive diffusion clearance on the sinusoidal membrane; PS_{bile}, intrinsic biliary clearance; CL_{met}, intrinsic metabolic clearance; Fa, fraction absorbed; k_a, absorption rate constant.

Subscripts. B, blood; LU, lung; BR, brain; MU, muscle; R, kidney; GI, gastrointestinal tract; H, liver; HE, liver extracellular space; inf, influx; met, metabolism.

Model Equations

Hepatic uptake, biliary excretion, and metabolic clearances in humans were linear parameters.

Blood pool:

$$V_B(dC_B/dt) = Q_{LU}(C_{LU}/K_{p,LU} - C_B) - CL_RC_B$$

Lung:

$$V_{LU}(dC_{LU}/dt) = Q_{BR}C_{BR}/K_{p,BR} + Q_{MU}C_{MU}/K_{p,MU} + Q_RC_R/K_{p,R} + Q_HC_{HE5} - Q_{LU}C_{LU}/K_{p,LU}$$

Brain, muscle, kidney:

$$V_i(dC_i/dt) = Q_i(C_B - C_i/K_{p,i})$$

Liver 1 to 5:

(1) rat $(V_{Hi}/5)(dC_{Hi}/dt) = (V_{m,inf}/5)f_BC_{HEi}/(K_{m,inf} + f_BC_{HEi}) + (PS_{dif}/5)f_BC_{HEi} - (PS_{dif}/5)f_TC_{Hi} - (V_{m,bile}/5)f_TC_{Hi}/(K_{m,bile} + f_TC_{Hi}) - (V_{m,met}/5)f_TC_{Hi}/(K_{m,met} + f_TC_{Hi})$

(2) human $(V_{Hi}/5)(dC_{Hi}/dt) = (PS_{inf}/5)f_BC_{HEi} + (PS_{dif}/5)f_BC_{HEi} - (PS_{dif}/5)f_TC_{Hi} - (PS_{bile}/5)f_TC_{Hi} - (CL_{met}/5)f_TC_{Hi}$

Liver extracellular compartment 1:

(1) rat $(V_{HE1}/5)(dC_{HE1}/dt) = Q_H(C_B - C_{HEi}) - (V_{m,inf}/5)f_BC_{HEi}/(K_{m,inf} + f_BC_{HEi}) - (PS_{dif}/5)f_BC_{HEi} + (PS_{dif}/5)f_TC_{Hi}$

(2) human $(V_{HE1}/5)(dC_{HE1}/dt) = Q_H(C_B - C_{HEi}) - (PS_{inf}/5)f_BC_{HEi} - (PS_{dif}/5)f_BC_{HEi} + (PS_{dif}/5)f_TC_{Hi} + k_aF_oX_{GI}$

Liver extracellular compartments 2 to 5:

(1) rat $(V_{HEi}/5)(dC_{HEi}/dt) = Q_H(C_{HE(i-1)} - C_{HEi}) - (V_{m,inf}/5)f_BC_{HEi}/(K_{m,inf} + f_BC_{HEi}) - (PS_{dif}/5)f_BC_{HEi} + (PS_{dif}/5)f_TC_{Hi}$

(2) human $(V_{HEi}/5)(dC_{HEi}/dt) = Q_H(C_{HE(i-1)} - C_{HEi}) - (PS_{inf}/5)f_BC_{HEi} - (PS_{dif}/5)f_BC_{HEi} + (PS_{dif}/5)f_TC_{Hi}$

Bile or gastrointestinal tract:

(1) rat $X_{bile} = \Sigma((V_{m,bile}/5)f_TC_{Hi}/(K_{m,bile} + f_TC_{Hi}))$

(2) human $X_{GI} = \Sigma(PS_{bile}/5)f_TC_{Hi} - (k_aFa)X_{GI}$

Appendix II: Effect of Renal Clearance on the Impact of the Change in the Uptake Clearance on the AUC of the Plasma and Liver

Q_h and CL_r represent the hepatic blood flow and renal clearance, respectively. PS_{inf}, PS_{eff}, and CL_{int} are hepatic uptake, sinusoidal efflux, and intrinsic sequestration clearances, respectively. V and C represent volume and concentration, respectively. Subscripts b, i, and h represent blood, inlet, and liver, respectively. Mass balance differential equations for each compartment in the simple model shown in Fig. 8 are as follows:

$$V_b \cdot \frac{dC_b}{dt} = Q_h(C_i - C_b) - CL_r \cdot C_b$$

$$V_i \cdot \frac{dC_i}{dt} = Q_h(C_b - C_i) - f_b \cdot PS_{inf} \cdot C_i + f_h \cdot PS_{eff} \cdot C_h$$

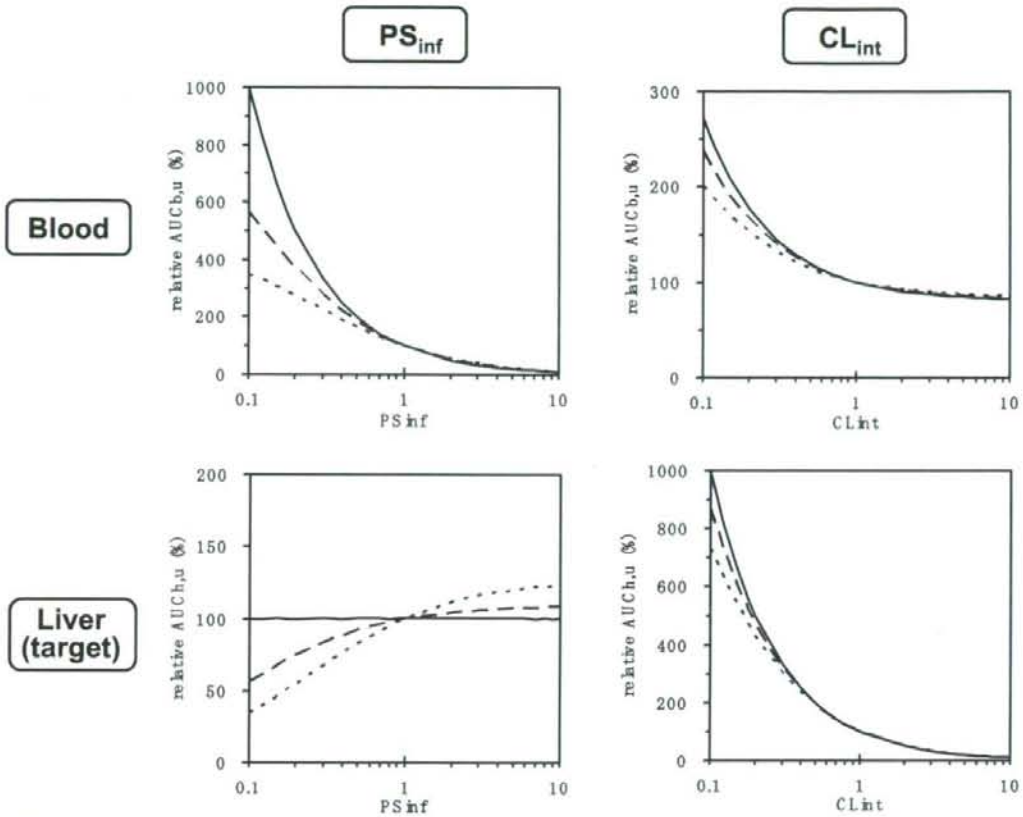

Fig. 9. Effects of renal clearance on the impact of changes in hepatic uptake and intrinsic sequestration clearances on the AUC of pravastatin in the blood and liver. Relative AUC (100% as the initial value) were estimated by varying the uptake and intrinsic sequestration clearances over a 0.1- to 10-fold range of the initial value when the renal clearance was 0 (——), 4 (– – –), and 16 (· · · · · ·) ml/min/kg.

$$V_h \cdot \frac{dC_h}{dt} = f_b \cdot PS_{inf} \cdot C_i - f_h \cdot (PS_{eff} + CL_{int}) \cdot C_h$$

Integrating these equations gives:

$$\frac{\text{Dose}}{f_b \cdot AUC_b} = \frac{PS_{inf} \cdot CL_{int}}{PS_{eff} + CL_{int}} \cdot \frac{CL_r + Q_h}{Q_h} + \frac{CL_r}{f_b} \quad \text{(A1)}$$

$$\frac{\text{Dose}}{f_h \cdot AUC_h} = CL_{int} + \frac{Q_h \cdot CL_r}{CL_r + Q_h} \cdot \frac{PS_{eff} + CL_{int}}{f_b \cdot PS_{inf}} \quad \text{(A2)}$$

where AUC_b and AUC_h represent the area under the concentration-time curve for the blood and liver, respectively. Substituting $CL_R = 0$ yields:

$$\frac{\text{Dose}}{f_b \cdot AUC_b} = PS_{inf} \cdot \frac{CL_{int}}{PS_{eff} + CL_{int}} \quad \text{(A3)}$$

$$\frac{\text{Dose}}{f_h \cdot AUC_h} = CL_{int} \quad \text{(A4)}$$

Equations A3 and A4 indicate that AUC_h depends only on CL_{int} when the renal clearance is negligible. In contrast, AUC_b is inversely proportional to PS_{inf}. If the renal clearance is maximal, that is, the renal blood flow (Q_r), eq. A2 can be converted to:

$$\frac{\text{Dose}}{f_h \cdot AUC_b} = CL_{int} + Q \cdot \frac{PS_{eff} + CL_{int}}{f_b \cdot PS_{inf}} \quad \text{(A5)}$$

where

$$Q = \frac{Q_h \cdot Q_r}{Q_r + Q_h} \approx 9$$

When the hepatic uptake is the rate-limiting process, so $CL_{int} \gg PS_{eff}$, eq. A5 can be converted to:

$$R = \frac{\text{Dose}}{f_h \cdot AUC_h} = CL_{int}\left(1 + Q \cdot \frac{CL_{int}}{f_b \cdot PS_{inf}}\right) \quad \text{(A6)}$$

In accordance, the R value can be higher than CL_{int} by up to $Q \times CL_{int}/(f_b \times PS_{inf})$. Figure 9 shows the effects of renal clearance on the impact of the changes in hepatic uptake and intrinsic sequestration clearance on the AUC of pravastatin in the plasma and liver. A simulation was performed using eqs. A1 and A2 and the parameters shown in Tables 1 and 2,

when the renal clearance was 0, 4 (one quarter of the renal blood flow), and 16 (the renal blood flow) ml/min/kg b.wt.

Acknowledgments

We thank Ayako Takada and Yuji Sekiya for excellent technical assistance.

References

Davies B and Morris T (1993) Physiological parameters in laboratory animals and humans. *Pharm Res* **10:**1093–1095.

Ghibellini G, Vasist LS, Leslie EM, Heizer WD, Kowalsky RJ, Calvo BF, and Brouwer KL (2007) In vitro-in vivo correlation of hepatobiliary drug clearance in humans. *Clin Pharmacol Ther* **81:**406–413.

Giacomini KM and Sugiyama Y (2005) Membrane transporters and drug response, in *Goodman & Gilman's The Pharmacological Basis of Therapeutics* (Brunton LL, Lazo JS, and Parker KL eds), 11th ed, pp 41–70, McGraw-Hill, New York.

Hasegawa M, Kusuhara H, Sugiyama D, Ito K, Ueda S, Endou H, and Sugiyama Y (2002) Functional involvement of rat organic anion transporter 3 (rOat3; Slc22a8) in the renal uptake of organic anions. *J Pharmacol Exp Ther* **300:**746–753.

Ishigami M, Tokui T, Komai T, Tsukahara K, Yamazaki M, and Sugiyama Y (1995) Evaluation of the uptake of pravastatin by perfused rat liver and primary cultured rat hepatocytes. *Pharm Res* **12:**1741–1745.

Iwatsubo T, Hirota N, Ooie T, Suzuki H, Shimada N, Chiba K, Ishizaki T, Green CE, Tyson CA, and Sugiyama Y (1997) Prediction of in vivo drug metabolism in the human liver from in vitro metabolism data. *Pharmacol Ther* **73:**147–171.

Jones HM, Parrott N, Jorga K, and Lavé T (2006) A novel strategy for physiologically based predictions of human pharmacokinetics. *Clin Pharmacokinet* **45:**511–542.

Kawai R, Lemaire M, Steimer JL, Bruelisauer A, Niederberger W, and Rowland M (1994) Physiologically based pharmacokinetic study on a cyclosporin derivative, SDZ IMM 125. *J Pharmacokinet Biopharm* **22:**327–365.

Kawai R, Mathew D, Tanaka C, and Rowland M (1998) Physiologically based pharmacokinetics of cyclosporine A: extension to tissue distribution kinetics in rats and scale-up to human. *J Pharmacol Exp Ther* **287:**457–468.

Kitazawa E, Tamura N, Iwabuchi H, Uchiyama M, Muramatsu S, Takahagi H, and Tanaka M (1993) Biotransformation of pravastatin sodium: I. Mechanisms of enzymic transformation and epimerization of an allylic hydroxy group of pravastatin sodium. *Biochem Biophys Res Commun* **192:**597–602.

Kivistö KT and Niemi M (2007) Influence of drug transporter polymorphisms on pravastatin pharmacokinetics in humans. *Pharm Res* **24:**239–247.

Komai T, Kawai K, Tokui T, Tokui Y, Kuroiwa C, Shigehara E, and Tanaka M (1992) Disposition and metabolism of pravastatin sodium in rats, dogs and monkeys. *Eur J Drug Metab Pharmacokinet* **17:**103–113.

Lennernäs H and Fager G (1997) Pharmacodynamics and pharmacokinetics of the HMG-CoA reductase inhibitors: similarities and differences. *Clin Pharmacokinet* **32:**403–425.

Link E, Parish S, Armitage J, Bowman L, Heath S, Matsuda F, Gut I, Lathrop M, and Collins R (2008) SLCO1B1 variants and statin-induced myopathy: a genome-wide study. *N Engl J Med* **359:**789–799.

Maeda K, Ieiri I, Yasuda K, Fujino A, Fujiwara H, Otsubo K, Hirano M, Watanabe T, Kitamura Y, Kusuhara H, et al. (2006) Effects of organic anion transporting polypeptide 1B1 haplotype on pharmacokinetics of pravastatin, valsartan, and temocapril. *Clin Pharmacol Ther* **79:**427–439.

Miyauchi S, Sawada Y, Iga T, Hanano M, and Sugiyama Y (1993) Comparison of the hepatic uptake clearances of fifteen drugs with a wide range of membrane permeabilities in isolated rat hepatocytes and perfused rat livers. *Pharm Res* **10:**434–440.

Morimoto K, Oishi T, Ueda S, Ueda M, Hosokawa M, and Chiba K (2004) A novel variant allele of OATP-C (SLCO1B1) found in a Japanese patient with pravastatin-induced myopathy. *Drug Metab Pharmacokinet* **19:**453–455.

Nakagomi-Hagihara R, Nakai D, and Tokui T (2007) Inhibition of human organic anion transporter 3 mediated pravastatin transport by gemfibrozil and the metabolites in humans. *Xenobiotica* **37:**416–426.

Nakai D, Nakagomi R, Furuta Y, Tokui T, Abe T, Ikeda T, and Nishimura K (2001) Human liver-specific organic anion transporter, LST-1, mediates uptake of pravastatin by human hepatocytes. *J Pharmacol Exp Ther* **297:**861–867.

Naritomi Y, Terashita S, Kimura S, Suzuki A, Kagayama A, and Sugiyama Y (2001) Prediction of human hepatic clearance from in vivo animal experiments and in vitro metabolic studies with liver microsomes from animals and humans. *Drug Metab Dispos* **29:**1316–1324.

Niemi M, Pasanen MK, and Neuvonen PJ (2006) SLCO1B1 polymorphism and sex affect the pharmacokinetics of pravastatin but not fluvastatin. *Clin Pharmacol Ther* **80:**356–366.

Niinuma K, Kato Y, Suzuki H, Tyson CA, Weizer V, Dabbs JE, Froehlich R, Green CE, and Sugiyama Y (1999) Primary active transport of organic anions on bile canalicular membrane in humans. *Am J Physiol* **276:**G1153–G1164.

Nishizato Y, Ieiri I, Suzuki H, Kimura M, Kawabata K, Hirota T, Takane H, Irie S, Kusuhara H, Urasaki Y, et al. (2003) Polymorphisms of OATP-C (SLC21A6) and OAT3 (SLC22A8) genes: consequences for pravastatin pharmacokinetics. *Clin Pharmacol Ther* **73:**554–565.

Obach RS (1999) Prediction of human clearance of twenty-nine drugs from hepatic microsomal intrinsic clearance data: an examination of in vitro half-life approach and nonspecific binding to microsomes. *Drug Metab Dispos* **27:**1350–1359.

Rane A, Wilkinson GR, and Shand DG (1977) Prediction of hepatic extraction ratio from in vitro measurement of intrinsic clearance. *J Pharmacol Exp Ther* **200:**420–424.

Roberts MS and Rowland M (1986) Correlation between in-vitro microsomal enzyme activity and whole organ hepatic elimination kinetics: analysis with a dispersion model. *J Pharm Pharmacol* **38:**177–181.

Sawada Y, Hanano M, Sugiyama Y, and Iga T (1985) Prediction of the disposition of nine weakly acidic and six weakly basic drugs in humans from pharmacokinetic parameters in rats. *J Pharmacokinet Biopharm* **13:**477–492.

Shitara Y, Horie T, and Sugiyama Y (2006a) Transporters as a determinant of drug clearance and tissue distribution. *Eur J Pharm Sci* **27:**425–446.

Shitara Y, Itoh T, Sato H, Li AP, and Sugiyama Y (2003) Inhibition of transporter-mediated hepatic uptake as a mechanism for drug-drug interaction between cerivastatin and cyclosporin A. *J Pharmacol Exp Ther* **304:**610–616.

Shitara Y and Sugiyama Y (2006b) Pharmacokinetic and pharmacodynamic alterations of 3-hydroxy-3-methylglutaryl coenzyme A (HMG-CoA) reductase inhibitors: drug-drug interactions and interindividual differences in transporter and metabolic enzyme functions. *Pharmacol Ther* **112:**71–105.

Singhvi SM, Pan HY, Morrison RA, and Willard DA (1990) Disposition of pravastatin sodium, a tissue-selective HMG-CoA reductase inhibitor, in healthy subjects. *Br J Clin Pharmacol* **29:**239–243.

Soars MG, Grime K, Sproston JL, Webborn PJ, and Riley RJ (2007) Use of hepatocytes to assess the contribution of hepatic uptake to clearance in vivo. *Drug Metab Dispos* **35:**859–865.

Takane H, Miyata M, Burioka N, Shigemasa C, Shimizu E, Otsubo K, and Ieiri I (2006) Pharmacogenetic determinants of variability in lipid-lowering response to pravastatin therapy. *J Hum Genet* **51:**822–826.

Yamaoka K, Tanigawara Y, Nakagawa T, and Uno T (1981) A pharmacokinetic analysis program (multi) for microcomputer. *J Pharmacobiodyn* **4:**879–885.

Yamazaki M, Akiyama S, Ni'inuma K, Nishigaki R, and Sugiyama Y (1997) Biliary excretion of pravastatin in rats: contribution of the excretion pathway mediated by canalicular multispecific organic anion transporter. *Drug Metab Dispos* **25:**1123–1129.

Yamazaki M, Akiyama S, Nishigaki R, and Sugiyama Y (1996a) Uptake is the rate-limiting step in the overall hepatic elimination of pravastatin at steady-state in rats. *Pharm Res* **13:**1559–1564.

Yamazaki M, Kobayashi K, and Sugiyama Y (1996b) Primary active transport of pravastatin across the liver canalicular membrane in normal and mutant Eisai hyperbilirubinemic rats. *Biopharm Drug Dispos* **17:**607–621.

Yamazaki M, Suzuki H, Hanano M, Tokui T, Komai T, and Sugiyama Y (1993) $Na^{(+)}$-independent multispecific anion transporter mediates active transport of pravastatin into rat liver. *Am J Physiol* **264:**G36–G44.

Yamazaki M, Tokui T, Ishigami M, and Sugiyama Y (1996c) Tissue-selective uptake of pravastatin in rats: contribution of a specific carrier-mediated uptake system. *Biopharm Drug Dispos* **17:**775–789.

Zhang W, Chen BL, Ozdemir V, He YJ, Zhou G, Peng DD, Deng S, Xie QY, Xie W, Xu LY, et al. (2007) SLCO1B1 521T→C functional genetic polymorphism and lipid-lowering efficacy of multiple-dose pravastatin in Chinese coronary heart disease patients. *Br J Clin Pharmacol* **64:**346–352.

Address correspondence to: Dr. Yuichi Sugiyama, Department of Molecular Pharmacokinetics, Graduate School of Pharmaceutical Sciences, University of Tokyo, 7-3-1 Hongo, Bunkyoku-Tokyo 113-0033, Japan. E-mail: sugiyama@mol.f.u-tokyo.ac.jp

Bull. Natl. Inst. Health Sci., **126**, 104-110 (2008) **Notes**

病院情報システムを用いた医療用医薬品による副作用の検出に関するパイロット研究

頭金 正博[#], 齋藤充生, 石黒昭博[*1], 三宅真二, 鈴木美和子[*2], 折井孝男[*2], 長谷川 隆一

Pilot Study of Data Collection System for Adverse Reactions of Prescribed Medications using Hospital Information Systems

Masahiro Tohkin[#], Mitsuo Saito, Akihiro Ishiguro[*1], Shinji Miyake, Miwako Suzuki[*2], Takao Orii[*2], Ryuichi Hasegawa

We attempted to establish an efficient information data collection system for very low frequent adverse drug reactions using a hospital information system. We collected the prescription data of all patients treated with statins at the Kanto Hospital from the drug order system. At the same time, we surveyed the laboratory data on rhabdomyolysis (creatine kinase) and kidney functions (creatinine and blood and urine nitrogen) of all the patients from examination order system. Thereafter, we collated the prescription data and the laboratory data to prepare a time-series table of medications and laboratory data for each patient. We extracted patients who showed abnormal increase of the serum creatine kinase from the time-series tables and analyzed the correlations between the increase in the serum creatine kinase and the dosage, kidney functions, age, or gender. From these results, we concluded that this information data collection system was useful for the post-marketing surveys of the incidence of adverse reactions occurring at a very low frequency.

Keywords: adverse drug reactions, hospital information system, rhabdomyolysis, statin

1. 緒言

スタチン系薬剤は高脂血症の治療薬として汎用されているが，副作用（薬剤の有害反応）として横紋筋融解症を発症する場合がある．発症頻度は極めて稀であるが，一旦発症すると副作用としては重篤であり，死亡する場合もある．しかし，スタチン系高脂血症薬による横紋筋融解症の発症機構については，ほとんど明らかにされておらず，医薬品の開発段階で横紋筋融解症の発症リスクを評価し，服用前に発症を予防することは現状では極めて困難である[1]．したがって，スタチン系薬剤の副作用に関するリスクを推定するためには，市販後のスタチン系高脂血症薬による横紋筋融解症の発症頻度などを正確に把握することが重要になる．しかし，横紋筋融解症は極めて稀にしか発症しないことから，スタチン系薬剤による横紋筋融解症の発症頻度に関する正確なデータを収集するためには，数万人以上の服用患者を確保する必要があり，そのためには膨大な労力と経費や時間が必要となる．このような状況は，極めて稀にしか発生しない副作用の調査には共通した課題となっており，市販後の医薬品に対する迅速な安全対策を実施する上での問題となっていることから，迅速で安価な調査方法の開発が望まれている．

ところで，我が国における病院情報システムの普及率は年々増加しており，全国規模での調査によると，600床以上の病院を対象とした場合は，平成17年度で4分の1以上にのぼり，大規模病院での入院・外来患者数を考慮するとかなりの症例数を集めることが期待できる[2]．病院情報システムは，各病院の医療状況に合わせて病院毎にカスタマイズしたシステムが用いられている場合が多く，その仕様や操作方法はシステムのプラットフォーム毎に異なっており，データの内容や扱い方も当然異なっているものの，我が国の医療環境や健康保険システムに適合させるために，共通な仕様となっている部分もある[3]．そこで，病院情報システムの共通仕様機能を用い

To whom correspondence should be addressed: Masahiro Tohkin; 1-18-1 Kamiyoga Setagaya-ku, Tokyo 158-8501, Japan; Tel: 03-3700-1141 ext567; Fax 03-3700-9788; E-mail: tohkin@nihs.go.jp

*1 (独) 医薬品医療機器総合機構安全部（医薬安全科学部・協力研究員）

*2 NTT東日本 関東病院薬剤部

て，医薬品の使用状況と副作用の発生状態についての汎用性のある調査システムが構築できれば，全国を対象とした副作用調査が，比較的安価で迅速に実施できる可能性がある．

以上のような考えにもとづいて，我々はスタチン系高脂血症薬を服用している患者を対象に，病院情報システムに保存されているスタチン系高脂血症薬の使用状況と横紋筋融解症に関連した検査値および腎機能，年齢，性別などの患者背景因子を網羅的に収集し，稀にしか発症しない副作用の発症頻度や患者背景因子との関係を調査する方法を開発することを目的とし，NTT東日本関東病院（関東病院）の病院情報システムの薬剤データ等を用いてパイロット研究を行った．

2．調査研究方法

2－1．関東病院での調査対象

関東病院で収集された研究対象者（被験者）の処方情報と検査値情報は匿名化された後に国立医薬品食品衛生研究所・医薬安全科学部へ電子データとして提供され，横紋筋融解症に関連した解析に用いられた．

(1) 調査対象

関東病院に入院・外来のリポバス（シンバスタチン），メバロチン（プラバスタチン），リピトール（アトルバスタチン），ローコール（フルバスタチン），リバロ（ピタバスタチン），クレストール（ロスバスタチン）のいずれかを服用している患者

(2) 調査対象期間

平成19年１月～平成19年６月

(3) 調査項目

(i) 患者背景

年齢，性別

(ii) 対象薬剤の使用状況

投与薬剤名，一日投与量，投与期間，処方せん発行日

(iii) 横紋筋融解症に関連した臨床検査値

血清クレアチンキナーゼ値（CK）

(iv) 腎機能に関連した臨床検査値

血清クレアチニン値（Cre），血中尿素窒素値（BUN），検査実施日

(4) 同意取得について

当研究は人体から採取された試料を用いない，既存資料等のみを用いる後ろ向き観察研究であり，全ての診療情報が資料提供機関で匿名化されることから，研究対象者からは，インフォームド・コンセントの取得は行わない（疫学研究に関する倫理指針「第７項　研究対象者からインフォームド・コンセントを受ける手続き等，(2)観察研究を行う場合　②人体から採取された試料を用いない場合」および「第11項　他の機関等の資料の利用，(2)既存資料等の提供にあたっての措置」参照）．なお，研究参加医療機関で研究対象となる可能性のある患者へは，当研究が実施されることを広報し周知させる努力を払った．また，本研究は国立医薬品食品衛生研究所・研究倫理審査委員会により，調査方法等について審査を受け実施が許可されている（受付番号145）．

2－2．関東病院でのスタチン系高脂血症薬の服用患者における血清クレアチンキナーゼ値上昇に関する調査

関東病院の病院情報システムは，電子診療録（電子カルテ）システムを中心に，診療支援，外来，患者サービス，薬剤支援，経営管理・物流，入院の各システムが連携している．処方システムと臨床検査システムは，電子診療録（電子カルテ）システムの中のオーダリングシステムに含まれるが，各オーダリングシステムは独立している．したがって，スタチン系高脂血症薬の服用患者の使用状況，検査値，入院・外来期間等のデータを病院情報システム上で患者単位のデータとして一括して検索・抽出することはできない．そこで，それぞれのシステムのデータセットから匿名化患者記号を指標にして抽出し，マイクロソフト・エクセルでスタチン系高脂血症薬の処方オーダー情報と検査値オーダーを統合する事にした．具体的な方法はFig.１に示す手順で患者情報の抽出と統合を行った．まず，調査期間内にスタチン系高脂血症薬処方オーダー歴のある患者データを診療系オーダーシステムから抽出し，匿名化患者記号，投与回数，投与日数，処方せん発行日等のデータを抽出する．期間内に１人の患者が複数回のスタチン系高脂血症薬の処方を受けているので，匿名化患者記号を指標にしてマイクロソフト・エクセルを用いて患者一覧表を作成し，重複する匿名化患者記号を１個の記号に統合し，時系列でスタチ

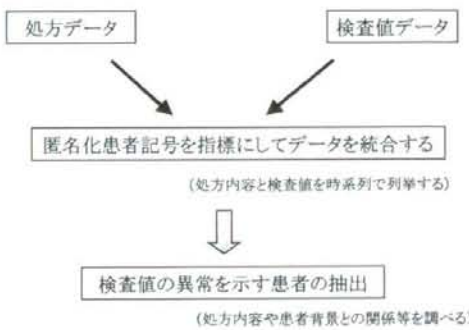

Fig. 1 Flow chart for the combination of prescription data and laboratory data

Table 1 Examples of prescription data, laboratory data, and time-series table

(A) Prescription data

薬品名	匿名化患者記号	処方日	処方量	日数
クレストール錠 2.5mg	abcdefgh	4/4	1	35
クレストール錠 2.5mg	bsdefghi	4/5	1	35
クレストール錠 2.5mg	cdefghijk	4/9	1	35
クレストール錠 2.5mg	defhijkl	4/9	1	28
クレストール錠 2.5mg	efghijklm	4/9	1	28
クレストール錠 2.5mg	fghijklmn	4/9	1	35
クレストール錠 2.5mg	ghijklmno	4/10	1	35
クレストール錠 2.5mg	hijklmnop	4/10	1	42
クレストール錠 2.5mg	ijklmnopq	4/11	1	68
クレストール錠 2.5mg	klmnopqr	4/11	1	35
クレストール錠 2.5mg	lmnopqrs	4/12	1	28
クレストール錠 2.5mg	mnopqrst	4/15	1	56
クレストール錠 2.5mg	nopqrstu	4/15	2	60
クレストール錠 2.5mg	opqrstuv	4/15	1	35
クレストール錠 2.5mg	pqrstuvw	4/16	1	56
クレストール錠 2.5mg	qrstuvwx	4/16	2	35
クレストール錠 2.5mg	rstuvwxy	4/16	1	56
クレストール錠 2.5mg	stuvwxyz	4/16	1	28
クレストール錠 2.5mg	tuvwxyza	4/17	1	20
クレストール錠 2.5mg	uvwxyzab	4/17	1	56
クレストール錠 2.5mg	vwxyzabc	4/18	1	76

(B) Laboratory data

検査日	匿名化患者記号	検査項目	結果値
4/1	wxyzabcd	Cre	1.33
4/1	wxyzabcd	BUN	22.00
4/1	wxyzabcd	CK	47.00
4/1	zabcdefg	Cre	0.47
4/1	zabcdefg	BUN	17.80
4/1	zabcdefg	CK	30.00
4/1	abcdefgh	Cre	0.99
4/1	abcdefgh	BUN	11.50
4/1	abcdefgh	CK	44.00
4/1	bsdefghi	Cre	1.40
4/1	bsdefghi	BUN	24.30
4/1	bsdefghi	CK	13.00
4/1	cdefghijk	Cre	1.56
4/1	cdefghijk	BUN	30.40
4/1	cdefghijk	CK	477.00
4/1	defhijkl	Cre	0.54
4/1	defhijkl	BUN	7.50
4/1	defhijkl	CK	58.00
4/1	efghijkl	Cre	0.80
4/1	efghijkl	BUN	20.50

(C) Time-series table of medications and laboratory data for each patient

abcdefgh	処方日	1/10	2/14	3/14	4/17	5/15	6/12	検査日	2/14	3/14				
	処方量	1	1	1	1	1	1	CK	81.00	76.00				
	日 数	35	28	28	28	28	28	Cre	0.69	0.70				
								BUN	11.60	15.00				
bsdefghi	処方日	1/16	3/6	6/12				検査日	1/16	3/6	6/12			
	処方量	1	1	1				CK	164.00	142.00	177.00			
	日 数	56	98	98				Cre	0.56	0.58	0.61			
								BUN	18.20	14.90	17.20			
cdefghijk	処方日	6/15						検査日	1/5	1/5	2/13	2/13	4/13	6/15
	処方量	1						CK	157.00	158.00	167.00	180.00	355.00	191.00
	日 数	56						Cre	0.83	0.83	0.87	0.87	0.86	0.90
								BUN	25.90	26.50	18.90	19.50	20.50	15.30
defhijkl	処方日	1/9						検査日	1/9	2/13	3/13	4/24	5/29	
	処方量	1	1	1	1	1		CK	152.00	148.00	80.00	142.00	247.00	
	日 数	35	28	42	35	28		Cre	2.00	2.34	1.90	2.01	2.11	
								BUN	43.60	36.30	31.10	37.00	51.70	
efghijklm	処方日	1/15						検査日	1/15					
	処方量	1	1	1				CK	132.00					
	日 数	56	90	97				Cre	1.04					
								BUN	14.80					
fghijklmn	処方日	2/27						検査日	2/27	5/28				
	処方量	1	1					CK	70.00	73.00				
	日 数	90	98					Cre	0.91	1.04				
								BUN	15.50	24.00				
ghijklmno	処方日	1/23						検査日	1/23	2/27	3/27	5/1		
	処方量	1	1	1	1			CK	Blank	122.00	157.00	144.00		
	日 数	35	28	35	35			Cre	0.67	0.68	0.70	0.69		
								BUN	Blank	14.10	14.20	11.70		

ン系高脂血症薬の処方状況を整理した（Table 1 (A)）．一方，検査系オーダーシステムから調査期間内の全ての患者についての今回の調査に必要な，CKやBUN，Cre等の臨床検査値を全て抽出し，臨床検査値一覧表を作成した（Table 1 (B)）．マイクロソフト・エクセルを用いて，スタチン系高脂血症薬の服用患者一覧表と臨床検査値一覧表を統合し，患者毎のスタチン系高脂血症薬の投与状況と検査値の変動を時系列で表示した（Table 1 (C)）．

2－3．全国規模でのスタチン系高脂血症薬の使用実態調査

日本病院薬剤師会が実施した調査で病院情報システムを導入していると報告した医療機関のうち300床以上の医療機関（204施設）を対象にして，平成17年度のスタチン系高脂血症薬の処方数量をアンケート方式で調べ集計した．

3．調査結果

3－1．スタチン系高脂血症薬の使用実態

関東病院の全ての入院・外来患者のうち平成19年1月～平成19年6月までの6ヶ月間でスタチン系高脂血症薬を投与された患者の総数は4,086名であった．各スタチン系高脂血症薬の使用患者数ではリピトールがもっとも多く，ついで，メバロチンが多く処方されていた（Table 2）．一方，ローコールの処方患者数は少なく73名のみであった．使用薬剤構成比について，平成17年度に実施した全国の204施設を対象とした調査結果（Fig. 2）と比較すると，関東病院での使用状況はリピトールの使用量が比較的多い点とローコールの使用量が少ない点が全国的な平均と異なっていた．関東病院でのクレストールの使用量が多いのは調査年の影響と思われる．

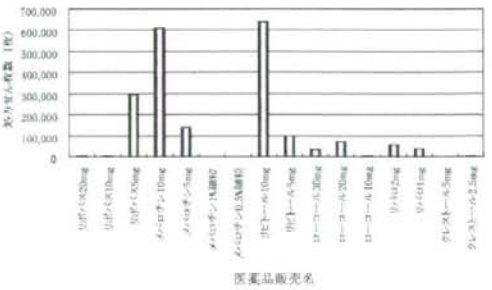

Fig. 2　Number of prescriptions for statins in the nation-wide 204 medical institutions

3－2．血清クレアチンキナーゼ値異常患者の頻度

スタチン系高脂血症薬服用患者4086名のうち，血清クレアチンキナーゼ（CK）値が500 IU/L以上の高値を示す患者は122名であった（Table 2）．また，薬剤毎のCK値が高値の患者数を集計したところ，今回調査した中では，クレストール，ローコール，リバロの頻度が高かった（Table 2）．

次に，各製薬企業が市販後等に調査したCK値の異常の頻度について，添付文書やインタビューフォームに記載している数字を調査し，Table 3にまとめた．また，関東病院で調査したCK高値（500 IU以上）の頻度と，添付文書等に記載されていた頻度をFig. 3に示した．その結果，今回の調査から得られた頻度の数字は添付文書に記載されている数字の2～3倍程度であったが，各薬剤での頻度の順はリピトールを除いて添付文書でのCK上昇の順と一致した．リピトールの添付文書に記載されている頻度については，調査母数が他の薬剤に比べて少

Table 2　Number of patients showing high values of creatine kinase and kidney function

医薬品販売名	患者総数	CK上昇＊		腎機能検査値異常				CK&腎機能検査値異常‡	
				Cre上昇＊＊		BUN上昇†			
	（人）	（人）	（%）	（人）	（%）	（人）	（%）	（人）	（%）
クレストール	207	9	4.3	27	13	52	25.1	6	2.9
ローコール	73	3	4.1	3	4.1	13	17.8	0	0.0
リバロ	288	12	4.2	32	11	61	21	8	3
リピトール	2118	71	3.4	244	12	512	24	43	2
リポバス	431	10	2.3	37	9	96	22	4	1
メバロチン	969	17	1.8	97	10	206	21	10	1
合　計	4086	122	－	440	－	940	－	71	－
平　均	－	－	3.3	－	9.7	－	22	－	1.6

＊　CK値が500 IU/L以上の示す患者
＊＊ Cre値が1.2 mg/dL以上の示す患者
†　BUN値が20 mg/dL以上の示す患者
‡　CK上昇症例のうちCreもしくはBUNも上昇した症例

Table 3 Information of creatine kinase and kidney function, which are described in the package inserts of statins

#	医薬品販売名	CK値上昇	Cre値上昇	BUN値上昇
1	クレストール	国内・外の臨床試験（承認時）：1.6%（171/10380例） 使用成績調査（2007年2月報告時）：2.3%（201/8795例）	記載なし	記載なし
2	ローコール	カプセル剤の承認時まで及び市販後2002年２月までの集計:1.5%（93/6368例）	0.1～5%未満	0.1～5%未満
3	リバロ	0.1%～2.0% ※インタビューフォーム：1.6%（323/20888例）	0.1%未満	0.1%未満
4	リピトール	５%以上 ※インタビューフォーム：6%（54/893例）	記載なし	頻度不明
5	リポバス	治験（2.5～10mg/日投与）：4.2%（42/1002例） 用量拡大治験（5～20mg/日投与）：5.5%（29/531例） 使用成績調査（第4年次迄の累計：5～10mg/日投与）：0.8%（65/8123例）	記載なし	0.1～5%未満
6	メバロチン	0.1～１%未満 ※インタビューフォーム：0.5%（61/11137例）	0.1%未満	0.1%未満

特記ない場合、「その他の副作用」の項において記載されている頻度に関する情報を示す

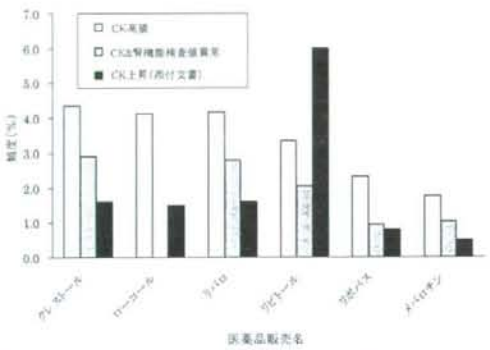

Fig. 3 Frequencies of patients showing high values of creatine kinase and abnormal kidney function
Frequencies of patients who showed high values of creatine kinase and abnormal kidney function are cited from this survey results and from package insert of statins

Table 4 Dosage of statins in patients showing high values of creatine kinase

医薬品販売名	投与量（CK値：>500発現時）				
	患者数				
クレストール錠	2.5mg				不明*
	3				6
ローコール錠	30mg				不明*
	3				0
リバロ錠	1mg	2mg	4mg		不明*
	1	1	2		8
リピトール錠	5mg	10mg	20mg		不明*
	19	14	1		37
リポバス錠	5mg	10mg	不明*		
	7	3			0
メバロチン錠	5mg	10mg	20mg	40mg	不明*
	2	4	1	1	9

不明*は調査開始時に既にCK値が高値を示していたため、投与量を特定できなかった

ないことから，市販後調査ではなく，治験のデータである可能性がある（Table３）.

３－３．血清クレアチンキナーゼ高値と患者背景要因との関係

CK 値の上昇と患者側の要因との関係を調べるため，スタチン系高脂血症薬の投与量および投与患者の腎機能を調べた．投与量については，Table４に示したように，同じスタチン系高脂血症薬での異なった投与量とCK 上昇患者数の関係を調べたところ，CK値が高値を示す以前の投与量のデータが今回の調査期間に含まれないために，投与量を特定できない場合が多かったが，投与量が特定可能であった症例では，投与量が多い場合でも必ずしもCK上昇患者数が多いとはいえなかった．また，腎機能との関係を調べるために，CK 上昇患者での血清クレアチニン値（Cr）と血清尿素窒素（BUN）を測定し，基準値（Cr>1.2 あるいはBUN>20）以上を示す腎機能が低下した患者数を集計し頻度を計算した（Table２）．CK値が高値を示す患者のうち腎機能が低下した患者数についても集計した（Table２）．その結果，薬剤によってはCK 高値患者の中に腎機能の低下している患者が高い割合で含まれている場合もあったが，今回の調査の範囲では腎機能が低下した時期とCK値が上昇した時期の関係が必ずしも明確でなく，腎機能とCK 上昇との明確な関係は不明であった．

スタチン系高脂血症薬の投与患者のうち，65歳以上の患者のみを高齢者患者群として抽出しCK値および腎機能検査値を集計したところ，高齢者患者群では腎機能の低下を示す患者の割合はスタチン系高脂血症薬の投与患

者全体に比べて増加しているものの，CK値の高値を示す患者割合は全体と差はなかった（Table 5）．また，投与患者を性別で集計した場合は，腎機能の低下を示す患者の割合は男女で差はなかったが，CK値の高値を示す患者の割合は男性の方が多かった（Table 6）．

4．考察

本研究ではパイロット研究として，関東病院における病院情報システムのデータソースから，匿名化患者記号を指標とし，スタチン系高脂血症薬の使用患者と臨床検査データを汎用ソフトであるマイクロソフト・エクセル

Table 5 Number of elderly patients showing high values of creatine kinase and abnormal kidney function

65歳以上（高齢者）

医薬品販売名	患者総数	CK上昇*		腎機能検査値異常				CK&腎機能検査値異常‡	
				Cre上昇**		BUN上昇†			
	（人）	（人）	（%）	（人）	（%）	（人）	（%）	（人）	（%）
クレストール	70	4	5.7	18	25.7	29	41.4	3	4.3
ローコール	42	1	2.4	2	4.8	9	21.4	0	0.0
リバロ	138	6	4.3	26	19	44	32	6	4
リピトール	1151	37	3.2	171	15	370	32	31	3
リポバス	298	5	1.7	28	9.4	73	24.5	2	0.7
メバロチン	620	10	1.6	78	13	165	27	7	1
合　計	2319	63	－	323	－	690	－	49	－
平　均	－	－	2.9	－	14.4	－	29.2	－	2.2

* CK値が500 IU/L以上の示す患者
** Cre値が1.2 mg/dL以上の示す患者
† BUN値が20 mg/dL以上の示す患者
‡ CK上昇症例のうちCreもしくはBUNも上昇した症例

Table 6 Number of patients showing high values of creatine kinase and abnormal kidney function in each gender

男性

医薬品販売名	患者総数	CK上昇*		腎機能検査値異常				CK&腎機能検査値異常‡	
				Cre上昇**		BUN上昇†			
	（人）	（人）	（%）	（人）	（%）	（人）	（%）	（人）	（%）
クレストール	106	7	6.6	17	16.0	24	22.6	5	4.7
ローコール	42	2	4.8	2	4.8	7	16.7	0	0.0
リバロ	186	9	4.8	29	16	44	24	6	3
リピトール	1355	55	4.1	189	14	326	24	30	2
リポバス	217	7	3.2	30	13.8	56	25.8	4	1.8
メバロチン	468	10	2.1	67	14	108	23	5	1
合　計	2374	90	－	334	－	565	－	50	－
平　均	－	－	3.8	－	13.4	－	22.4	－	2.2

女性

医薬品販売名	患者総数	CK上昇*		腎機能検査値異常				CK&腎機能検査値異常‡	
				Cre上昇**		BUN上昇†			
	（人）	（人）	（%）	（人）	（%）	（人）	（%）	（人）	（%）
クレストール	101	2	2.0	10	9.9	28	27.7	1	1.0
ローコール	31	1	3.2	1	3.2	6	19.4	0	0.0
リバロ	102	3	2.9	3	3	17	17	2	2
リピトール	763	16	2.1	55	7	186	24	13	2
リポバス	214	3	1.4	7	3.3	40	18.7	0	0.0
メバロチン	501	7	1.4	50	6	98	20	5	1
合　計	1712	32	－	106	－	375	－	21	－
平　均	－	－	2.1	－	5.3	－	20.4	－	0.9

* CK値が500 IU/L以上の示す患者
** Cre値が1.2 mg/dL以上の示す患者
† BUN値が20 mg/dL以上の示す患者
‡ CK上昇症例のうちCreもしくはBUNも上昇した症例

を用いて統合し，全てのスタチン系高脂血症薬の服用患者から横紋筋融解症のマーカーであるCK値が高値を示す患者を抽出し，薬剤毎のCK上昇の患者発症頻度を算出することが可能であることを示した．今回の調査から算出した発症頻度と添付文書に記載されているCK値の上昇の頻度については，各薬剤間の相対的な傾向はほぼ一致していた．したがって，我々の考案した病院情報システムを使用した医薬品の使用状況と副作用の発生状態についての調査システムについては，病院情報システムのプラットフォームが異なっていても実施可能であり，算出した発症頻度についてもほぼ満足できる数字であることが明らかになった．市販後の医薬品における副作用の調査としては，薬事法に基づく副作用報告のデータを用いた調査がある．副作用報告に基づくデータは全ての市販されている医薬品を対象にしている点や全国を網羅している点で優れたデータであるものの，使用者総数は集計されていないため頻度を算出することができない．その他にも，製薬企業が実施する市販後調査があり，データの正確性などで優れているが，実施される品目が限られている点や，公表されるまでに時間がかなり経過するなどの点で問題がある．また，諸外国で行われる健康保険データを用いる調査などがあるが，我が国では今のところ健康保険データは公開されていない．以上の調査方法に比べて，我々の考案した調査方法は，病院情報システムを稼働させている病院の協力が得られれば，データの正確性，経費，調査期間のいずれにおいても優れた方法であると考えられる．

スタチン系高脂血症薬の服用患者でのCK値の上昇と患者背景要因との関係を調べるために，スタチン系高脂血症薬の投与量と患者の腎機能との関係を精査した．CK値が高値を示す以前の投与量と腎機能のデータが今回の調査期間に含まれないために投与量を特定できない場合があったが，CK値が高値を示した時期での投与量や腎機能が特定可能であった症例では，今回の調査の範囲では，両者ともCK値上昇との明確な関係は不明であった．患者の生理機能との関係を調べる場合は，CK値上昇との時期的な関係を長期間に渡って明らかにすることが必要であると思われた．また，他病院からの紹介をうけた患者などで初診時に既にCK値が高値を示した場合などは，背景因子との関係を検討する対象としては適さないと考えられた．

今回調査対象としたスタチン系高脂血症薬のほとんどの添付文書には「高齢者で横紋筋融解症があらわれやすいとの報告がある」と記載されていることから，65歳以上の患者と全体で比較したところ，既に文献で報告されているように腎機能は高齢者患者群で低下していたが[4]，CK値の高値を示す患者の割合は全体と差はなかったことから，添付文書の記載については今回の結果から確認することはできなかった．また，男女でのCK値の高値を示す患者の割合を比較したところ，男性の方が高い頻度を示した．この結果から男性が筋障害を生じやすい可能性が考えられたが，男性のCK値の基準値が女性より高いことを反映している可能性も考えられた．

今回の調査は1施設でのデータを用いているために，一部のスタチン系高脂血症薬の使用状況が全国的レベルでのデータと異なっていたことや，入院・外来患者の特徴に偏りがある可能性があることから，横紋筋融解症やCK高値の発症頻度などは，今回の結果を単純に一般化することはできない．しかし，全国の医療機関をこの調査の対象にすることが可能であれば，薬剤毎の副作用の発生頻度のみならず，発症患者の背景因子との関係を解析することが可能になり，医薬品の市販後安全対策にとって，貴重なデータが得られるものと考える．

謝　辞

本研究を実施するに当たりましてご協力いただきました（社）日本病院薬剤師会に深謝いたします．

参考文献

1）横紋筋融解症．重篤副作用疾患別対応マニュアル第1集，日本医薬情報センター　2007年．
2）厚生労働省大臣官房統計情報部．平成17年患者調査．
3）医療マネジメント学会：電子カルテシステムの普及に向けて，じほう　2004年．
4）加藤隆一：薬の体内動態と年齢，臨床薬物動態学，南江堂　1998年．

In: Drugs: Approval and Evaluation, Delivery and Control ISBN: 978-1-60456-533-1
Editors: A.O. Hartmann, L.K. Neumann

Chapter 6

INVESTIGATION OF NEW MOLECULAR ENTITIES OF DRUGS APPROVED IN THREE REGIONS, JAPAN, US AND EU

Mitsuo Saito and Ryuichi Hasegawa
Division of Medicinal Safety Science, National Institute of Health Sciences,
Tokyo, Japan

ABSTRACT

The number of new molecular entities (NMEs) approved in 2006 was 20 in Japan, 24 in US and 25 in EU, respectively. Among 70 NMEs approved in both Japan and US and/or EU during 2002 to 2006, 69 NMEs had been approved in US and 35 in EU by 2006, and there was only one common approval solely between Japan and EU. On the other hand, 39 NMEs were solely approved in US and EU during this period. Among 109 NMEs approved in either two or three regions, the number of preceding NMEs was 3 in Japan, 85 in US and 21 in EU.

1. INTRODUCTION

In order to promptly supply medicinal products that are needed in medical practice, measures for improving the efficiency of the drug approval review system have been undertaken. In the present study, in order to clarify the situation of drug approval, an investigation was conducted for the circumstances of approval of medicinal products containing a new molecular entity (NME) in 2006 in the three regions: Japan, the US and the EU; and comparative analyses were also conducted for NMEs that were approved between 2002 and 2006.

2. Methods of Investigating the Circumstances of Approvals in the Three Regions

For the approval situation in Japan, we investigated review reports obtained from the website of the Pharmaceuticals and Medical Devices Agency (http://www.info.pmda.go.jp/shinyaku/shinyaku_index.html). Regarding the US, we extracted brand names of NMEs from the FDA's CDER Drug and Biologic Approval Reports (http://www.fda.gov/cder/rdmt/). We also examined approval history obtained from Drugs@FDA (http://www.accessdata.fda.gov/scripts/cder/drugsatfda/index.cfm). For the EU, we extracted brand names of NMEs through the Centralized Approval Process from the Community Register of medicinal products (http://ec.europa.eu/enterprise/pharmaceuticals/register/index.htm) provided by the European Commission, and investigated product overview on target drugs from the EMEA's EPARs for authorized medicinal products for human use (http://www.emea.europa.eu/htms/human/epar/a.htm).

Table 1. NMEs approved in Japan, US and EU in 2006

Japan	US	EU
Aripiprazole	Sunitinib	Daptomycin
Silodosin	Ranolazine	Human normal Ig
Letrozole	Lubiprostone	Galsulfase
Clopidogrel	Anidulafungin	Fentanyl
Follitropin Alfa	Decitabine	Pegaptanib
Cetrorelix	Varenicline	Rotigotine
Tolterodine	Rasagiline	Alglucosidase alpha
Sertraline	Darunavir	Tigecycline
Solifenacin	Dasatinib	Timolol
Gabapentin	Avobenzone	Parathyroid hormone
Mozavaptane	Ecamsule	Clofarabine
Temozolomide	Octocrylene	Rimonabant
Interferon Beta-1a	Posaconazole	Entecavir
Entecavir	Biskalcitrate	Natalizumab
Bortezomib	Vorinostat	Sorafenib
Ropinirole	Sitagliptin	Sunitinib
Remifentanil	Ciclesonide	Dexrazoxane
Perflubutane	Telbivudine	Antithrombin alfa
Agalsidase Alfa	Kunecatechins	Sitaxentan
Laronidase	Paliperidone	Perflutren
	Alglucosidase alfa	Deferasirox
	Ranibizumab	Buprenorphine
	Idursulfase	Varenicline
	Panitumumab	Exenatide
		Dasatinib